Size/Strain Diffraction Peak Broadening of the Energetic Materials FOX-7, RDX and ADN

Michael HERRMANN*, Ulrich FÖRTER-BARTH
and Paul Bernd KEMPA

*Fraunhofer Institut für Chemische Technologie,
J.-v.-Fraunhofer-Str. 7, 76327 Pfinztal, Germany*
E-mail: michael.herrmann@ict.fraunhofer.de

Abstract: X-ray powder diffraction (XRD) is an established tool for the investigation of energetic materials. Whereas positions and intensities of diffraction peaks yield information on the crystal structure, peak profiles are related to the real structure described by crystallite size, shape and microstrain. A series of energetic materials were measured at the synchrotron ANKA, and the size/strain broadening of FOX-7, RDX and ADN is discussed in relation to crystal structures and properties.

Keywords: X-ray diffraction, microstructure, FOX-7, RDX, ADN.

Introduction

The investigation of the crystal structure using X-ray diffraction is an established tool in research, development and quality assessment of energetic materials used for propellants and explosives. Besides, the real or microstructure shifted more and more within the scope of actual research, as it was shown that a careful modification of the crystalline load reduces the shock sensitivity of plastic bonded explosives (PBX). In this context particle size, shape, surface morphology, voids, inclusions, impurities, dislocations and twins are discussed to influence the mechanical sensitivity and the creation of Hot Spot during shock loading. For this reason, crystallite size and microstrain were investigated by means of X-ray diffraction, for example, of the cyclic nitramines RDX ($C_3H_6N_6O_6$) and HMX ($C_4H_8N_8O_8$) [1, 2]. The investigations correlate the size/strain broadening with particle processing and mechanical sensitivities.

Furthermore, anisotropic diffraction peak broadening was found for the energetic materials. On this base a series of energetic materials were measured at the synchrotron ANKA, and the broadening characteristics were evaluated in detail for various particle qualities.

X-ray Powder Diffraction and Evaluation Techniques

The diffraction patterns include three types of information: geometrical, structural and physical state. In powder patterns measured with monochromatic radiation geometrical information is contained in the angular positions of diffraction peaks and structural information in the peak intensities. The profiles of diffraction peaks represent the physical state of the sample and the measuring instrument. Their use for the investigation of microcrystalline properties is almost as old as the powder diffractometry itself. In 1918 Scherrer reported that the widths of diffraction lines are proportional to the inverse crystallite size and in 1925 Van Arkel found that lines are broadened by microstrain. Modern X-ray powder diffraction techniques are described, for example, by Klug & Alexander and by Chung & Smith [3, 4].

Two evaluation techniques for size/strain broadening of X-ray diffraction peaks are used in the following applications; the Double-Voigt approach [5] and the Williamson-Hall plot [6]. In the Double-Voigt approach crystallite size (domain size) and microstrain comprise Lorentzian and Gaussian component convolutions of diffraction peaks varying in the diffraction angle 2θ as a function of $1/cos\ \theta$ and $tan\ \theta$, respectively. Implemented into a whole pattern fit of the program TOPAS of Bruker AXS [7], the approach yields volume weighted mean crystallite sizes L_{Vol-IB} and a mean strain value $e_0\ (=\Delta d/d)$. For the method after Williamson and Hall, reciprocal peak widths $\beta^*=\beta/\lambda\ cos\ \theta$ are plotted versus reciprocal lattice distances $d^*=2/\lambda\ sin\ \theta$, where β, d, 2θ and λ are the diffraction line width, lattice distance, diffraction angle and wavelength of the radiation. If strain broadening is negligible, the β^*-values lie on a horizontal line with an intercept at the inverse of the mean linear crystallite size t. If size broadening is negligible, the values lie on a straight line through the origin with the integral breadth ξ of the strain contribution as slope, provided that microstrain is isotropic. The composite peak broadening produced by simultaneous small particle size and strain depends on the broadening functions of both effects.

In addition, Rietveld analysis was used for determining the concentration of HMX-impurities in RDX. Details of the method are described for example by Young in 1995 [8] or in the description of the program TOPAS [7].

Samples, Diffraction Experiments and Evaluation

A FOX-7 sample, four RDX samples, referred to in the following as RDX (1), RDX (2), RS-RDX and I-RDX, an ADN sample and the standard reference material lanthanum hexaboride were used for the X-ray diffraction investigations. FOX-7 and ADN (ground) was procured from Eurenco Bofors, RDX (2) and RS-RDX from Dyno Nobel ASA (class 5, each), I-RDX from Eurenco, Group SNPE, (M3C), and the standard reference material SRM 660a from the National Institute of Standards & Technology (NIST). RDX (1) is a processed sample. Median particles sizes of RDX (1), RDX (2), RS-RDX and I-RDX are ~5, 17.6, 9.7 and 10.5 μm, respectively.

The samples were measured at the diffraction beamline at ANKA on a Bragg-Brentano diffractometer equipped with a germanium analysator crystal and rotating sample holder using monochrome synchrotron radiation with wavelengths of 1.1479 and 1.2997 Å. Selected 2θ-ranges were measured with a step width of 0.0025°. Diffraction peaks were indexed using the program TOPAS from Bruker AXS and fitted using the split-Pearson VII analytical function yielding full widths at half maximum (FWHM). The peak widths of the energetic materials were reduced by geometric peak widths deduced from lanthanum hexaboride patterns, and the diffraction data were evaluated with Williamson-Hall plots. Besides, mean crystallite sizes and microstrains were refined using whole pattern fit, hkl-phases, fundamental parameters and the Double-Voigt approach of the program TOPAS [7], and the concentration of crystalline HMX impurities in RDX were determined by Rietveld-analysis. Since anisotropy may impact the separation of crystallite size and microstrain broadening, selected peak groups were evaluated separately, in addition to the whole pattern evaluation.

Results

The mean crystallite sizes L_{Vol-IB}, the mean strain values e_0 obtained by the Double-Voigt approach and the HMX-concentrations in RDX obtained from Rietveld analysis of the XRD pattern and by HPLC [14] are summarized in Table 1.

Table 1.   Size/strain values obtained by the Double-Voigt approach and HMX-content of RDX

Material	Description	Size	Strain	HMX-content [%]	
		L_{Vol-IB} [nm]	e_0	XRD	HPLC
FOX-7	all peaks	>3000	0.071		
	(hkl), k≠0	152	0.043		
	(h0l) trace	317	0.019		
RDX (1)	all peaks	244	0.045	4.7	6.5
	(h0l) trace	160	0.041		
	(hk0)trace	311	0.046		
RDX (2)		>3000	0.029	0.44	0.52*
RS-RDX		>3000	0.021	2.6	2.6*
I-RDX		>3000	0.023	0	0.01*
ADN		364	0.026		

* data reported by Gerber et al. [14]

FOX-7

FOX-7 crystallizes in the monoclinic space group $P2_1/n$; details of the crystal structure are reported by Bemm and Östmark [9]. Figure 1 depicts the Williamson-Hall plot of the FOX-7 sample; obviously the distribution is split into an approximately horizontal trace below 0.015 Å^{-1} and a widespread belt above 0.015 Å^{-1} (reciprocal peak widths). Indexing of the diffraction peaks of the horizontal trace revealed Miller indices (h0l) but (hkl) with k≠0 for the peaks which belong to the belt. Thus, the distribution represents a characteristic anisotropy, which is typical for stacking faults. When comparing the results with the crystal structure depicted in Figure 2, it becomes obvious that the (h0l) peaks of the trace represent the situation in the molecular layers, and the non-(h0l) peaks the directions crossing the layers.

The molecular layer structure is reported to be a model for low sensitivity materials, such as FOX-7 [9], FOX-12 [10] and TATB [11]. In this model the principal mechanism for release of mechanical load is layer slippage, which remains the internal layer structure undisturbed. The slip, however, would release only stress components parallel to the layers; stress components perpendicular would break layers. Further investigations of differently loaded samples shall show how the broadening characteristic will be affected by particle processing.
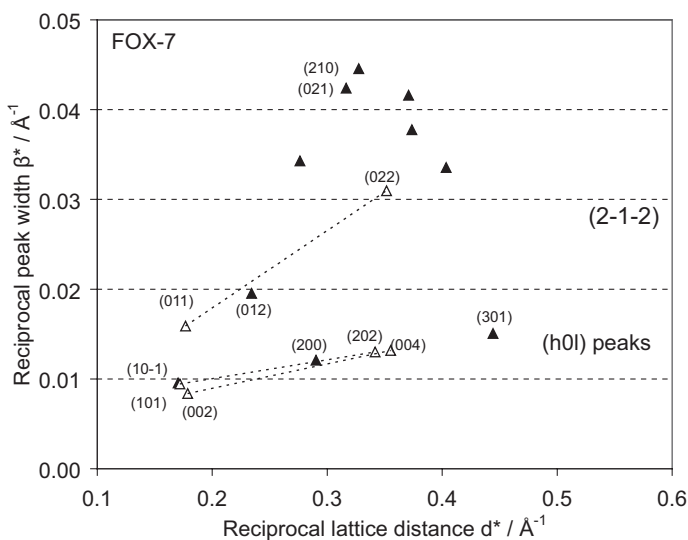
Figure 1. Williamson-Hall plot of FOX-7; low size/strain broadening of (h0l) peaks but strong broadening of (hkl) peaks with k ≠ 0. Higher-order relations of diffraction peaks are marked by unfilled triangles and dashed lines.
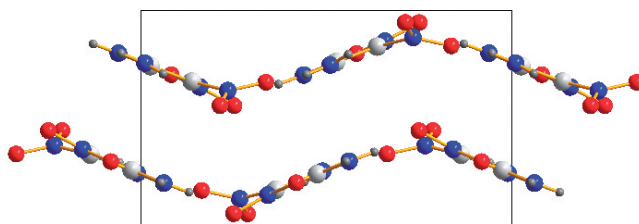

Figure 2. Layered crystal structure and unit cell of FOX-7; based on the data reported by Bemm [9]. Projection along a-axis, c-axis horizontal, b-axis upwards.

The size strain values of separately evaluated (h0l) and non-(h0l) peaks in Table 1 yielded domain sizes of 152 and 317 nm and microstrain values of 0.043 and 0.019 in and crossing the layers, respectively. An overall evaluation of all peaks yielded 4500 μm domain size, which principally means no size broadening. So far the Double-Voigt approach yielded different results, depending on whether anisotropy is taken into account or not. The results for (h0l) and non-(h0l) peaks are in coincidence with the anisotropic layer model and the Williamson-Hall plot.

RDX

RDX crystallizes in the orthorhombic space group Pbca; details of the crystal structure are reported by Choi and Prince in 1972 [12]. Figure 3 depicts the Williamson-Hall plot of a RDX sample (1) which contains 4.7 % HMX as impurity. The data point arrangement within a belt-like distribution starting above 0.01 Å^{-1} (reciprocal peak width). Higher-order relations of diffraction peaks are marked by unfilled triangles and dashed lines. The (h0l) and (hk0) peaks confine the distribution as upper and lower rims of the belt, where the (h0l) peaks are strongly and (hk0) peaks are weakly broadened. The measured peak width of (004) does not fit in this concept, most likely due to peak overlap.
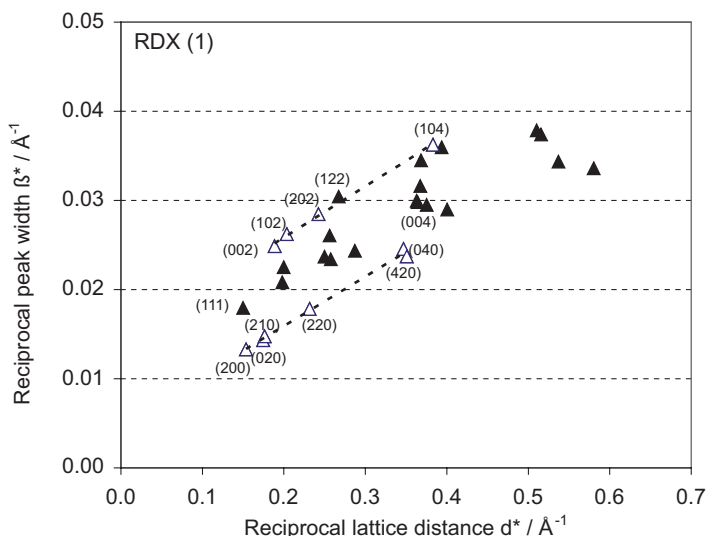

Figure 3.   Williamson-Hall plot of a RDX sample containing 4.7% HMX; belt-like distribution with low size/strain broadening of (hk0) peaks (unfilled triangles near lower dashed line), but strong broadening of (h0l) peaks (unfilled triangles near upper dashed line).

The crystal structure depicted in Figure 4 shows that, with the molecules far from being plane, the structure is more 3-dimensionally interwoven than FOX-7. No layer slip occurs on external stress but dislocation slip on two slip systems (010)[001] and {021}[100] (slip plane and Burgers vector) as reported by Gallagher et al. [13]. The peaks (002) and (020) indicate a comparably high size/strain broadening along the Burgers vector [001] but low broadening related to the slip plane (010). However, a detailed evaluation has still to be done.
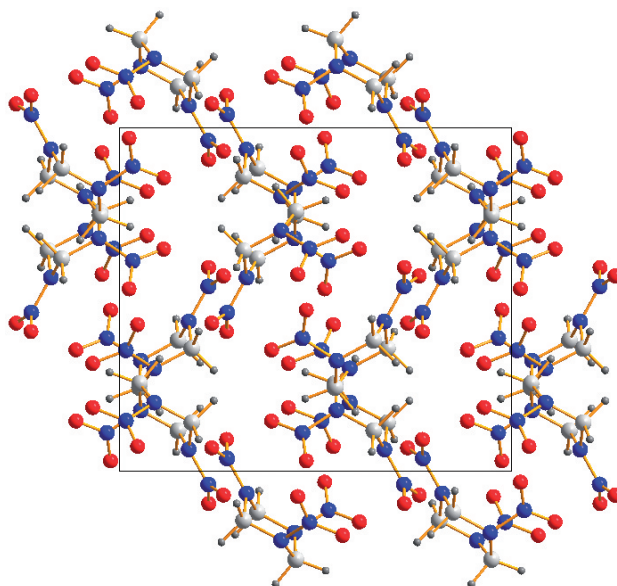
Figure 4. Crystal structure and unit cell of RDX; based on the data reported by Choi et al. [12]. Projection along c-axis, a-axis horizontal, b-axis upwards.
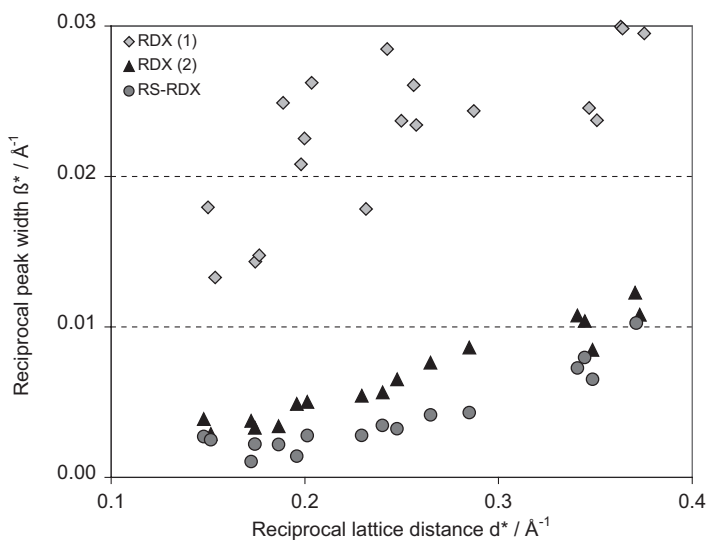

Figure 5. Williamson-Hall plot of RDX-varieties, including the HMX-containing sample RDX (1), a RDX (2) and a I-RDX, represented by diamonds, triangles and circles, respectively.

A comparison of various RDX qualities is shown in Figure 5, including the samples RDX (1), RDX (2), and I-RDX. Obviously, diffraction peak broadening and anisotropy of RDX (1) are much more pronounced, when compared to RDX (2) and I-RDX. Furthermore, the traces of the RDX (2) and I-RDX separate significantly, in particular between 0.2 and 0.35 1/Å reciprocal lattice distance; starting with the (002) peak, which is related to the Burgers Vector of the first slip system.

The size/strain parameters in Table 1 show a relatively high microstrain value of 0.045 and a domain size of 244 nm for RDX (1). A differentiated evaluation, which takes the anisotropy into account, revealed similar strain values of 0.041 and 0.046 but strongly anisotropic domain sizes varying from 160 to 311 nm for the (h0l) and (hk0) traces, respectively. The domain sizes of RDX (2) and the reduced sensitivity varieties RS-RDX and I-RDX are larger than 3 μm, and the strain values range between 0.02 and 0.03, where microstrain values of the reduced sensitivity varieties are 0.021 and 0.023 compared to 0.029 of RDX (2). So far the values of the Double-Voigt approach are coincident with the plots.

A further important parameter, the HMX-content, is also suggested to influence the crystal quality. Therefore, the HMX-contents determined by X-ray diffraction (XRD) and HPLC are included in Table 1. When comparing the data, it seems that the high HMX concentration of 6.5% in RDX (2) causes a poor crystal quality, but the lower concentration of 2.8% does not impact the crystal quality of RS-RDX. A comparison of the HMX-contents determined by X-ray diffraction (XRD) and HPLC [14] in the Table 1 provides an explanation. While HPLC yields the whole HMX-concentration, XRD records only that part which is crystallized in its own structure. Thus, the differences represent HMX which, for instance, is incorporated in the RDX lattice as guest molecules or as an amorphous part in grain boundaries. For RDX (1) and RDX (2) differences of 1.8 and 0.08% were found; the parts which most likely strain the RDX-lattice. No differences were found for the reduced sensitivity varieties, RS-RDX and I-RDX. Similar results were reported for coarse crystals using a rocking curve approach by Herrmann et al. in 2008. The investigations correlated low size/strain broadening with reduced shock sensitivities of PBX, but also showed that a low HMX-content is not a sufficient condition for high crystal quality and reduced sensitivity [15].

ADN

ADN crystallizes in the monoclinic space group $P2_1/c$; details of the crystal structure are reported by Gidaspov et al. in 1995 [16] and Gilardi et al. in 1997 [17]. Figure 6 shows the Williamson-Hall plot of ADN, where the higher-order relations of diffraction peaks are marked by unfilled triangles and dashed lines. The fluctuations and different slopes of the dashed lines indicate that anisotropy

is also an issue in ADN. However, broadening is moderate compared to FOX-7 or RDX (1); all values are below 0.02 Å^{-1} (reciprocal peak width). Figure 7 shows the crystal structure of the ion lattice using the data of Gilardi. Defect types of ADN are not yet reported in literature. The evaluation by the Double-Voigt approach yielded a relatively large domain size of 364 nm and a moderate microstrain value of 0.026.
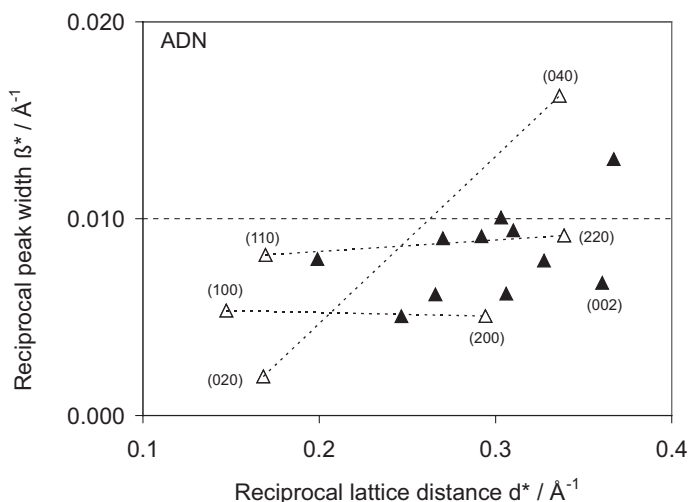

Figure 6.   Williamson-Hall plot of ADN. Higher-order relations of diffraction peaks are marked by unfilled triangles and dashed lines.
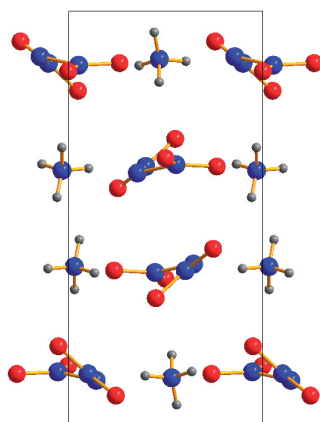

Figure 7.   Crystal structure and unit cell of ADN; based on the data reported by Gilardi et al. [17]. Projection along a-axis, c-axis horizontal, b-axis upwards.

Conclusions

The diffraction peak broadening of a series of energetic materials were investigated using synchrotron radiation. The use of size/strain broadening is well established for the investigation of metals with high symmetry and absorption, but proofed also to be a powerful tool for energetic material. Results of FOX-12, HMX and CL20 were recently reported [18], those of FOX-7, RDX and ADN are reported here. The method revealed valuable information on the real structure related to molecular shape, crystal structure, domain size, microstrain and defects such as stacking faults, dislocations and twinning. Crystal qualities of HMX and RDX samples were thus differentiated and correlated with its processing techniques and shock sensitivities. The results shall be used as a basis for future quality assessment.

References

[1] Herrmann M., Microstructure of Energetic Particles Investigated by X-ray Powder Diffraction, *Part. Part. Syst. Charact.*, **2005**, *22*, 401-406.

[2] Herrmann M., Kempa P.B., Doyle S., Microstructure of Energetic Crystals – Grain by Grain via Rocking Curve, *Z. Kristallogr. Suppl.*, **2007**, *26*, 557-562.

[3] Klug H.P., Alexander L.E., *X-ray Diffraction Procedures for Polycrystalline and Amorphous Materials*, John Wiley & Sons, New York **1974**.

[4] Chung F.H., Smith D.K., *Industrial Applications of X-Ray Diffraction*, Marcel Dekker, Inc., New York **2000**.

[5] Balzar D., Voigt Function Model in Diffraction-Line Broadening Analysis, in: (Snyder R.L., Bunge H.J., Fiala J., Eds.), *Microstructure Analysis from Diffraction*, Oxford University Press, **1999**.

[6] Williamson G.K., Hall W.H., X-ray Line Broadening from Filed Aluminium and Wolfram, *Acta Metall.*, **1953**, *V1*, 22-31.

[7] *Diffrac-plus, TOPAS V 2.1*, User's Manual, Bruker AXS, Karlsruhe, Germany **2003**.

[8] *The Rietveld Method*, (Young R.A., Ed.), IUCr, Oxford University Press, New York **1995**.

[9] Bemm U., Östmark H., 1,1-Diamino-2,2-dinitroethylen: a Novel Energetic Material with Infinite Layers in Two Dimensions, *Acta Cryst.*, **1998**, *C54*, 1997-1999.

[10] Östmark H., Bemm U., Bergman H., Langlet A., N-Guanylurea-Dinitramide:

a New Energetic Material with Low Sensitivity for Propellants and Explosives Applications, *Thermochim. Acta*, **2002**, *384*, 253-259.

[11] Stevens L.L., Velisavljevic N., Hooks D.E., Dattelbaum D. M., Hydrostatic Compression Curve for Triamino-Trinitrobenzene Determined to 13.0 GPa with Powder X-ray Diffraction, *Propellants Explos., Pyrotech.*, **2008**, *33*(4), 286-195.

[12] Choi C.S., Prince E., The Crystal Structure of Cyclotrimethylene-trinitramine, *Acta Cryst.*, **1972**, *B28*, 2857.

[13] Gallagher H.G., Halfpenny P.J., Miller J.C., Sherwood J.N., Dislocation Slip Systems in Pentaerythritol Tetranitrate (PETN) and Cyclomethylene Trinitramine (RDX), *Phil. Trans. R. Soc. Lond.*, **1992**, *A 339*, 293-303.

[14] Gerber P., Fuhr I., Mikonsaari I., Kretschmer A., Shock Wave Sensitivity of Charges Containing Insensitive Nitramine, *36th Int. Annu. Conf. of ICT*, **2005**, 139.1-10.

[15] Herrmann M., Förter-Barth U., Mathieu J., Patscheider J., Investigation of RS-RDX Samples from the MSIAC-Round Robin by Means of X-ray Diffraction Rocking Curves, *39th Int. Annu. Conf. of ICT*, **2008**, 57.1-6.

[16] Gidaspov B.V., Tselinskii I.V., Mel'nikov V.V., Margolis N.V., Grigor'eva N.V., Crystal and Molecular Structure of Dinitramide Salts and Acid-Base Properties of Dinitramide, *Russian Journal of General Chemistry*, **1995**, *65*(6), *Part 2,* 906.

[17] Gilardi R., Flippen-Anderson J., George C., Butcher R.J., A new Class of Flexible Energetic Salts: The Crystal Structures of the Ammonium, Lithium, Potassium, and Cesium Salts of Dinitramide, *J. Am. Chem. Soc.*, **1997**, *119*, 9411-9416.

[18] Herrmann M., Förter-Barth U., Kempa P. B., Size/strain diffraction peak broadening of the energetic materials HMX, CL-20 and FOX-12, *40th Int. Annu. Conf. of ICT*, **2009**, 32.1-11.